Structure, forming ability, and electrical-transport properties of isotypical amorphous alloys M_xSn_{1-x} (M=Fe,Co,Ni)

J.-F. Geny, G. Marchal, Ph. Mangin, Chr. Janot, and M. Piecuch
Laboratoire de Physique du Solide, Laboratoire Associé au Centre National de la Recherche Scientifique, N° 155, Faculté des Sciences—Case Officielle N° 140, 54037 Nancy-Cedex, France
(Received 14 August 1981)

Amorphous films of M_xSn_{1-x} (M=Fe,Co,Ni) have been prepared by vapor quenching over a wide range of composition. Interference functions have been obtained from electron diffraction, electrical-transport properties have been measured, and forming ability and stability have been studied. Chemical short-range order has been found to be very similar in the three condensed states of these alloys (amorphous, liquid, crystalline states) and the notion of isotypical structure has been extended to amorphous alloys. The forming ability of these metallic glasses has been correlated to the difficulties for these systems to accommodate too large a chemical disorder in crystalline phases.

I. INTRODUCTION

In the developing family of glassy metals, more and more amorphous alloys have been reported, and tentative classifications have been proposed.[1,2] One questionable point remains whether amorphous alloys may be found in as many different aspects as their crystallized counterparts; that is, do the following exist?

(1) Amorphous "solid solutions" with chemical species randomly distributed.

(2) The possibility of "miscibility gap" with formation of a mixture of two different amorphous phases in which each amorphous phase would exhibit its own chemical and topological short-range order.

(3) Intermetallic amorphous "compounds" available only in quite a restricted composition range with a "quasimolecular" short-range order characterized by rather weak fluctuations in nearest-neighbor surroundings and orientations of the chemical bondings.

In pursuing this further, one might wonder whether isotypy is still a reasonable notion in amorphous alloys; in other words, whether crystallized systems having similar equilibrium phase diagrams might be obtained in the amorphous state with the same chemical and topological short-range orders.

In this paper some data are reported concerning M_xSn_{1-x} amorphous alloys (with M=Fe,Co,Ni). The equilibrium phase diagrams of the corresponding crystallized systems can be considered as quite similar and exhibit only continuous changes through the M series. In particular, a number of isotypical intermediate compounds do exist, and if the notion may be extended to amorphous materials, such an illustration may be formed here.

In this paper emphasis is successively placed on the following.

(i) The determination of the compositional range of forming ability of the amorphous alloys, which is a different notion from their temperature range of stability as determined by the compositional dependence of the crystallization temperature T_{cr}.

(ii) The structural approach by comparing short-range order in amorphous, liquid, and crystallized materials.

(iii) The electrical resistivity behavior to be compared to that of liquid systems.

(iv) Finally, forming ability and stability of the M_xSn_{1-x} amorphous alloys are discussed in terms of general criteria.

II. EXPERIMENTAL PROCEDURES

A. Alloy preparation

In the present work the samples were prepared in an ultrahigh-vacuum chamber by simultaneous condensation on cooled substrates (77 K) of tin and transition metal (Fe, Co, or Ni) evaporated from thermal and electron beam crucibles, respectively. The pressure was better than 2×10^{-8} Torr during the evaporation process, the ultimate obtainable vacuum being 1×10^{-9} Torr. The evaporation rates were controlled and measured using two

 ©1982 The American Physical Society

quartz monitoring systems (QMS) whose vibration period is a linear function of the deposited mass. Thus the alloy composition can be determined after calibration of the QMS.

The substrates used were glass plates with preevaporated chromium-gold electrodes for resistivity measurements, optically polished glass plates for thickness and density data, and carbon-coated grids for electron microscopy investigations.

B. Resistivity measurements

In situ electrical resistance measurements were performed on films of about 500 Å thickness using a four-point probe method accurate to 0.01%. Resistivities are deduced from electrical resistance data after determination of the sample thicknesses using a Tolansky interferometric method. The accuracy of the procedure is better than 2%.

Five samples (10×10 mm^2) are simultaneously prepared, giving five differently composed alloys, due to an adequate geometrical distribution of the substrates each side of the mediator plan of the evaporation sources. Thus, reproducibility from experiment to experiment can easily be checked by slightly overlapping the composition ranges covered by the five samples of successive runs. Composition gradients within one sample are less than 1%.[3]

C. Electron microscopy and diffraction investigation

Electron micrographs and diffraction patterns have been obtained using a classical 100-keV electron microscope. As previously explained, the samples here are carbon-coated grids on which the alloys to be studied have been deposited. The diffraction patterns are photographically recorded. To ensure an accurate determination of the scattering wave vectors, a zone of the grids is deposited with a crystalline aluminum thin film which is then used as a standard for permanent wave-vector calibration without removing the grid from the microscope or changing focus.[4]

From these diffraction profiles, interference functions can be obtained through a procedure described elsewhere[5] assuming that the background contributions of inelastic scattering and Laue incoherent elastic scattering[6,7] are roughly the same in both amorphous and crystallized states for a given alloy. An iterative approach leads to the best interference functions $J(K)$ with a fairly good accuracy in the position of the intensity maxima and a reasonable qualitative description of the K dependence, but a rather poor estimate of the relative intensities ($\pm15\%$). Energy filters used to remove the large inelastic background would greatly improve the performance.[8]

D. Density measurements

As previously described,[9] the density of amorphous films can be obtained from the deposited mass as deduced from the calibrated QMS scale[10] and the film thickness as directly measured by a multiple-beam interferometric technique.[11] Thicknesses are determined with an error less than ±15 Å. Such a density determination is accurate to about $\pm2\%$.

III. FORMING ABILITY AND THERMAL STABILITY OF THE STUDIED AMORPHOUS ALLOYS; EXPERIMENTAL RESULTS

The resistivity of the as-quenched samples ρ_0 at 77 K and the resistivity changes upon thermal aging have been measured as explained in Sec. II B. A typical experimental resistivity behavior is shown in Fig. 1. Label 0 is applied to the as-quenched state and gives ρ_0. One-way irreversible paths such as $0\rightarrow1$, or $1\rightarrow3$, etc., correspond to thermal heating at a rate of 2 K/min from 77 K to T_1 or from T_1 to T_3, etc. Two-way reversible sequences $1\rightleftarrows2$, or $3\rightleftarrows4$, correspond to a thermal cycle between 77 K and T_1, or between 77 K and T_3, etc. These reversible changes are linear in T

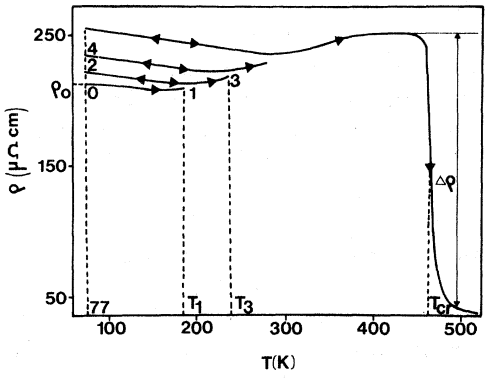

FIG. 1. Typical electrical resistivity behavior upon thermal heating treatment as explained in the text.

and roughly parallel; their slope gives the so-called temperature coefficient of the resistivity (TCR) $\alpha=(1/\rho)(d\rho/dT)$ which will be analyzed in a following section.

For a particular temperature T_{cr} an abrupt irreversible change $\Delta\rho$ in the resistivity is observed, which corresponds to crystallization. Thus one may reasonably speculate, from the resistivity behavior, that "structural defects" are present in the as-quenched amorphous alloys, with a more or less continuous distribution of activation energies or recovery temperatures. Warming up to T_i results in the annealing of the defects whose recovery temperature is smaller than T_i.

The resistivity changes $\Delta\rho$ at T_{cr} are mostly negative. However, $\Delta\rho$ is positive in Fe_xSn_{1-x} alloys with $x>0.37$.[12] Such an increase of the resistivity upon crystallization has already been reported in the Fe_xSi_{1-x} amorphous system[13] and can be related to the final product of crystallization changing with the composition of the initial amorphous alloy.

As long as $T_{cr}>\mathrm{RT}$ (room temperature) the samples can be removed from the preparation chamber before the onset of crystallization, and the structural state can be investigated by electron microscopy and diffraction. Such a systematic investigation has shown that when observed before a sharp-edged resistivity step the alloys are really in an amorphous state (continuous semidark electron micrographs and diffraction liquidlike patterns with broad diffuse rings), while they have become crystallized compounds after this resistivity step. Then, even when the sharp-edged resistivity step occurs at too low a temperature ($T_{cr}<\mathrm{RT}$) for the amorphous state to be checked through electron microscopy measurements, the corresponding T_{cr} temperature will be considered as a true crystallization temperature.

For M_xSn_{1-x} alloys with $x>x_s$ (x_s depending on the M element), the resistivity recovery upon crystallization is smeared out over a large temperature range (Fig. 2) which widens as x increases. Electron micrographs taken before the "crystallization stage" show the presence of small crystals (about 200-Å size) immersed in an amorphous pool. The T_{cr} stage corresponds to the transformation of this amorphous pool into crystals. Thus, x_s has to be considered as the true top forming ability limit for the M concentration in M_xSn_{1-x} amorphous alloys, and the compositional dependence of the crystallization temperature, as shown in Fig. 3, is relevant only for $x<x_s$. Note

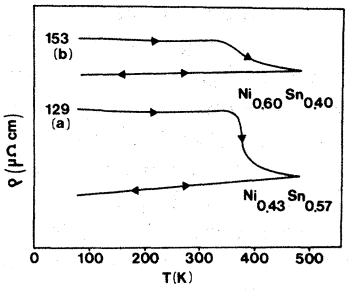

FIG. 2. Typical resistivity changes at crystallization for two Ni_xSn_{1-x} amorphous alloys. (a) $x<x_s$, (b) $x>x_s$.

that for Co_xSn_{1-x} alloys with $x>0.6$, the crystallization leads to a very small change of the resistivity. T_{cr} is poorly defined and determined by the use of the electron microscopy.

The compositional bottom limit x_I of forming ability is not as easily determined because the electron microscopy observations are not obtainable. The three $T_{cr}(x)$ curves seem to converge to the $x\simeq 0.1$ value, as if this particular M rate would be the lowest amount of impurities requested for tin metal to be obtained in the amorphous state. The same bottom limit has been reported for Cu_xSn_{1-x} amorphous alloys.[14] Thus, while the value of x_s seems to be imposed by the transition metal, x_I

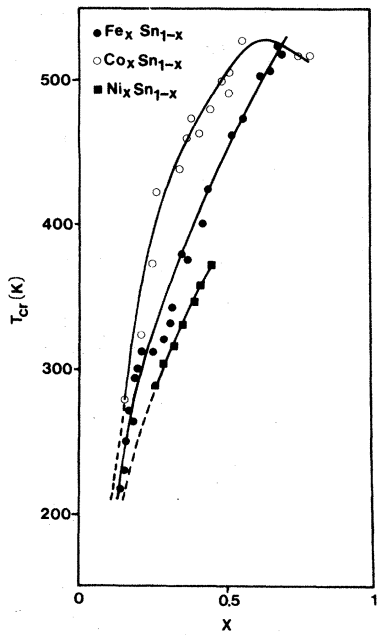

FIG. 3. Compositional dependence of the crystallization temperature of the Fe_xSn_{1-x} (●), Co_xSn_{1-x} (○), and Ni_xSn_{1-x} (■) amorphous alloys.

looks as if it were more typical of the tin element. The $T_{cr}(x)$ are increasing functions of the transition-metal content (Fig. 3) for a given system. The other features that must be pointed out are the large values of T_{cr} which reach 500 K in Fe_xSn_{1-x} and Co_xSn_{1-x} but remain smaller than 400 K in Ni_xSn_{1-x} and the fact that T_{cr} in Co_xSn_{1-x} is larger than in Fe and Ni alloys for a given composition despite the sequence order of Fe, Co, and Ni in the periodic table of the elements. The less stable and less feasible system happens to be Ni_xSn_{1-x}, while Co_xSn_{1-x} is more stable than Fe_xSn_{1-x}.

IV. STRUCTURAL APPROACH

A. Experimental data

Some preliminary results obtained from the Fe_xSn_{1-x} amorphous systems have been previously

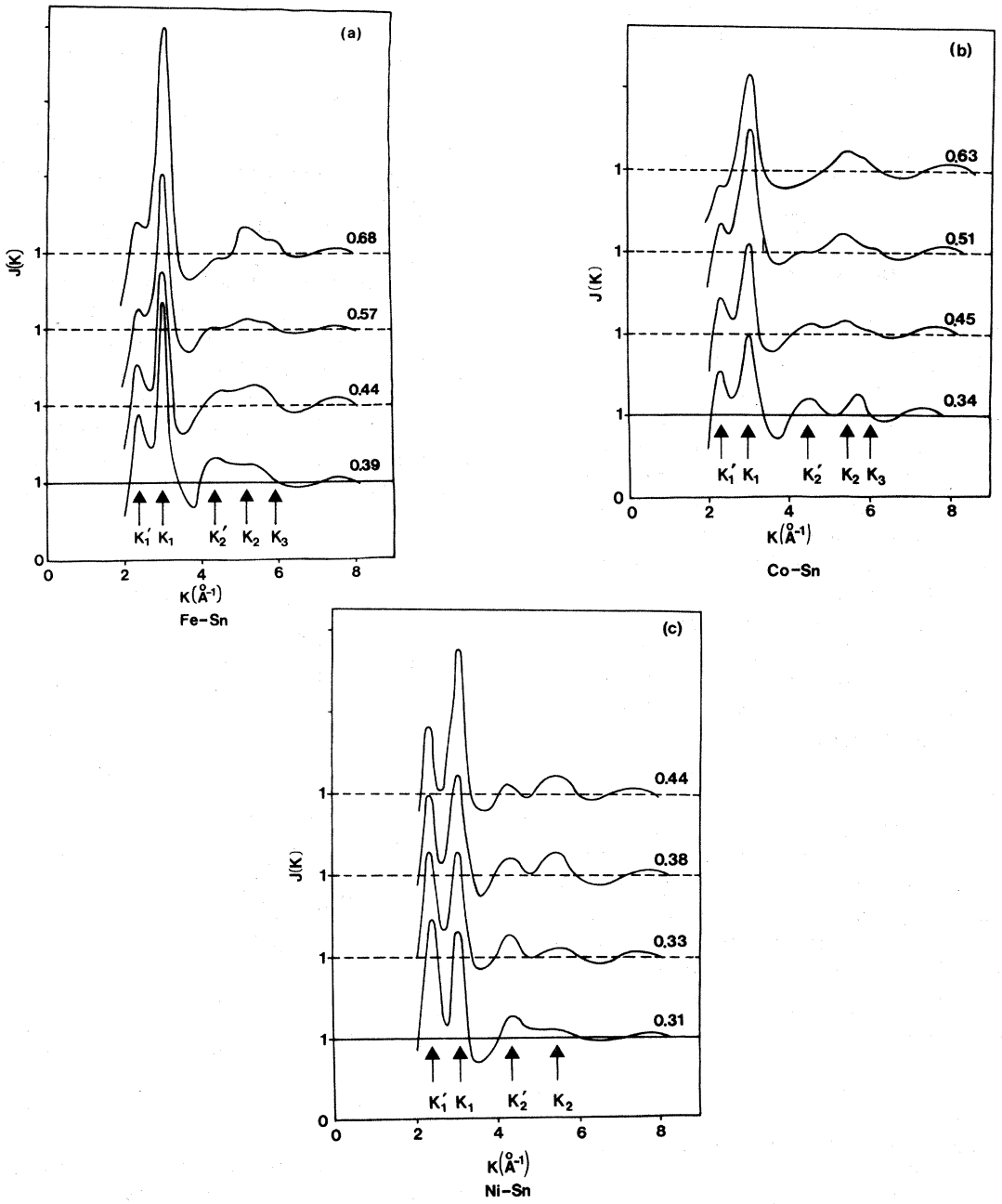

FIG. 4. Interference functions of the M_xSn_{1-x} amorphous alloys: $M=$(a) Fe, (b) Co, (c) Ni.

published.[15] In this paper, a complete set of interference functions have been recorded for the three systems M_xSn_{1-x} (M=Fe,Co,Ni). Some of them are shown in Fig. 4, from which the following features can be noted.

(i) For alloys having the largest content of transition metal, the interference functions are typical of a classical amorphous metal—a first intense maximum at K_1 and a weaker one at K_2, with a distinct shoulder at $K_3 > K_2 > K_1$.

(ii) Going to the tin-rich side results in the appearance, and then the growth, of two more peaks at positions K'_1 and K'_2. The K'_1 peak reaches an intensity comparable to that of the K_1 peak near the composition $x \approx 0.33$, and the intensity ratio $J(K'_1)/J(K_1)$ has a composition dependence not too far from that which can be expected when taking into account the tin and M atomic fractions and scattering factors (Fig. 5).

(iii) The position of the K_1 peaks is constant for a given system whatever the composition, and is shifted towards the large values when one goes from Fe to Ni through Co alloys. On the other hand, the K'_1 peak position is only slightly affected by the composition or the nature of the transition metal (Fig. 6).

Positions of the intensity maxima are reported in Table I along with data taken from the liquid CuSn system[16] and liquid tin.[17]

B. A comparison to near systems

Obvious similarities of the M_xSn_{1-x} interference functions with that of the CuSn liquid system[16]

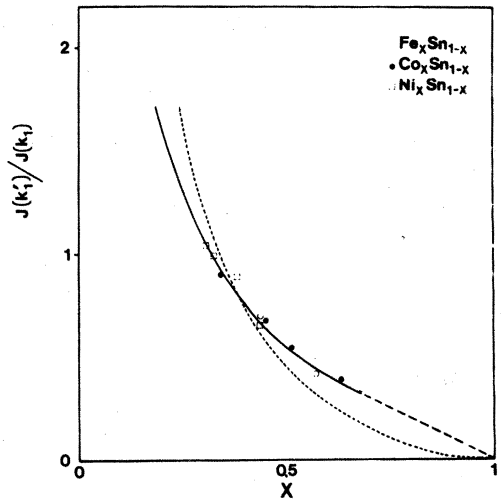

FIG. 5. Compositional dependence of $J(K'_1)/J(K_1)$ compared to calculated values $1.85\,(1-x^2)/[x^2+3.3x(1-x)]$.

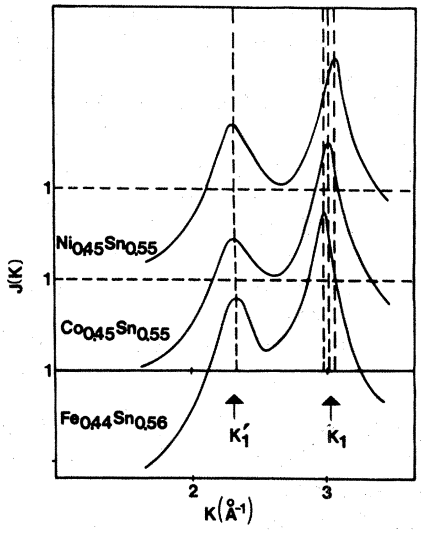

FIG. 6. Details of Fig. 4 near the first maxima of the interference functions.

can be observed by comparing the patterns shown in Figs. 4 and 7(a): a large maximum near $K_1 \simeq 3$ Å^{-1} on the M- or Cu-rich side and the appearance and growth of two peaks at $K'_1 \simeq 2.3$ Å^{-1} and $K'_2 \simeq 4.35$ Å^{-1} when the tin concentration increases. As shown in the partial interference functions[18] [Fig. 7(b)], K'_1 and K'_2 correspond to the Sn-Sn correlations and are at the same position as that of the maxima of the pure liquid tin [Fig. 7(a)] interference function, while K_1 is not too far from the first maximum of the Cu-Cu and Cu-Sn correlations. As usual, the shoulder K_3 at the K_2 maximum, which is observed in the diffraction patterns of the M_xSn_{1-x} amorphous systems as well as with Cu-Sn amorphous alloys, does not exist for liquid Cu-Sn.[19]

From the reduced distribution function shown in Fig. 7(c), the interatomic distances in liquid Cu-Sn have been calculated[20] near the liquidus temperature, $d_{Cu-Cu}=2.60$ Å, $d_{Cu-Sn}=2.70$ Å, $d_{Sn-Sn}=3.14$ Å, and also at 1100 °C, $d_{Cu-Cu}=2.60$ Å, $d_{Cu-Sn}=2.67$ Å, $d_{Sn-Sn}=3.10$ Å. Again, $d_{Cu-Cu} \simeq d_{Cu-Sn}$, and d_{Sn-Sn} is very different.

C. A tentative approach to the structure of the M_xSn_{1-x} amorphous alloys

The first idea that can be considered from the experimental data and the comparison with results concerning the Cu-Sn system is that K_1 corre-

TABLE I. Positions of the main peaks in the interference functions of the M_xSn_{1-x} amorphous (am) alloys, compared to those of liquid (liq) tin (Ref. 17) and liquid Cu-Sn (Ref. 16).

System	K_1' (Å^{-1})	K_1 (Å^{-1})	K_2' (Å^{-1})	K_2 (Å^{-1})	K_3 (Å^{-1})	K_2/K_1	K_3/K_1
am-Fe-Sn	2.35	2.96	4.32	5.20	5.85	1.76	1.98
am-Co-Sn	2.33	3.02	4.40	5.37	6.00	1.78	1.99
am-Ni-Sn	2.36	3.06	4.33	5.45		1.78	
liq-Sn	2.30		4.30				
liq-Cu-Sn	2.30	3.00	4.30	5.00		1.67	

sponds to the confused first maxima of the $J_{M\text{-}M}$ and $J_{M\text{-}Sn}$ partial interference functions while K_1' and K_2' belong to $J_{Sn\text{-}Sn}$.

Such an idea is quite well supported by considerations of the crystalline structure exhibited by the corresponding equilibrium systems. These crystalline structures[21–23] belong to the following three "families."

(i) C 16 structure: $FeSn_2$, $CoSn_2$.

(ii) B 35 structure: CoSn; FeSn; $D0$ 19 structure: Ni_3Sn, Fe_3Sn; $B35+D019$ structure: Fe_3Sn_2.

(iii) "family": Co_3Sn_2, Ni_3Sn_2, Fe_5Sn_3, Cu_5Sn_6.

In the C 16 structure, a given M atom is surrounded by eight Sn atoms and two M atoms while one Sn has 11 Sn and 4 M in its nearest-neighbor

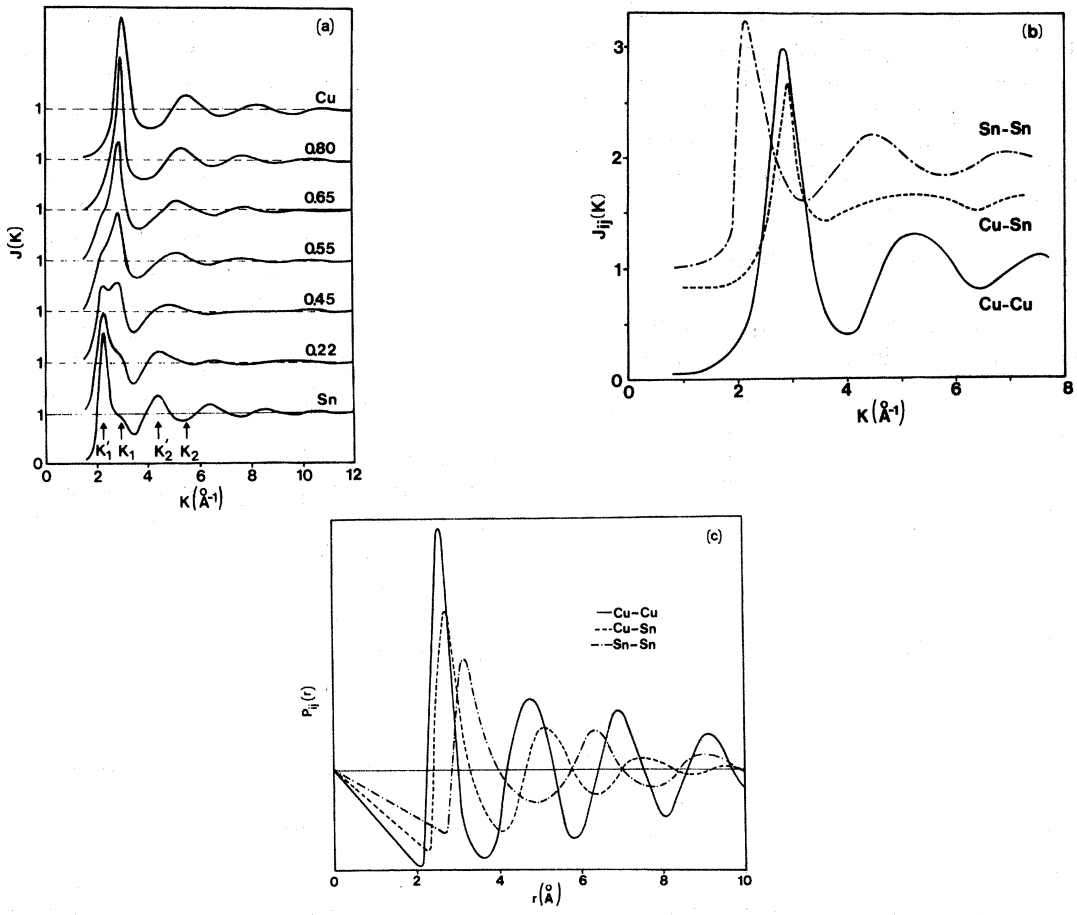

FIG. 7. (a) Total interference functions of liquid Cu-Sn alloy from Ref. 16. (b) Partial interference functions. (c) Partial reduced distribution function.

(NN) shell, with the following atomic distances: $d_{Fe\text{-}Fe}=2.66$ Å, $d_{Co\text{-}Co}=2.72$ Å, $d_{Fe\text{-}Sn}=2.79$Å, $d_{Co\text{-}Sn}=2.75$ Å, and $d_{Sn\text{-}Sn}$ ranges from 2.8 to 3.4 Å.

The three structures of family (ii) can be built by piling up *A* and *B* like planes of atoms. The *A* planes have a hexagonal close-packed structure with each iron atom surrounded by $4Fe+2Sn_I$, each tin atom having 6 Fe in its *n-n* plane shell. The *B* planes are hexagonal networks of Sn_{II} atoms. Then the *B* 35 structure is an *ABAB*... sequence, *D*0 19 corresponds to an *AAA*... sequence and Fe_3Sn_2 to a *BAABAAB*... with possible light distortion of the planes. As an example, local-order characteristics are given in Table II for various intermediate compounds of the Fe-Sn system.

One can see that the Fe-Sn and Fe-Fe distances are ranging over quite a narrow interval around 2.7 Å while the Sn-Sn distances are not too far from 3.1 Å. It is worth noting that the Sn_{II} sites center trigonal prisms of six iron atoms (see Fig. 8). Similar conclusion would be reached with Ni and Co compounds.

The structures belonging to the (iii) family are not so well established. They have been sometime described as modified *B* 8_1 or *B* 8_2 structures. An alternative description has been proposed by Malaman[23]: The Co_3Sn_2 and Ni_3Sn_2 compounds which have low-temperature stable forms would be derived from a *B* 35 structure by removing Sn_{II} atoms in half of the hexagonal cells (Fig. 8); the high-temperature stable phases, although less organized, would keep the principal of the *B* 35 or *D*0 19 structure, that is, practically the same distances between *M-M* and *M*-Sn atoms.

If the local surroundings of *M* atoms in the studied amorphous systems is supposed to be as close-packed as in their crystallized counterparts, one may expect to reach the *n-n* distances through the Ehrenfest relation $K_1d=7.89$ which reduces the interference function to the contribution of the NN shell. Doing that with the data given in Table I results in $d_{Fe\text{-}Fe}=d_{Fe\text{-}Sn}=2.65$ Å, $d_{Co\text{-}Co}=d_{Co\text{-}Sn}=2.61$ Å, $d_{Ni\text{-}Ni}=d_{Ni\text{-}Sn}=2.58$ Å.

When applied to tin atoms, the Ehrenfest relation gives $d_{Sn\text{-}Sn}=3.4$ Å, which is certainly too large a value since the validity of the Ehrenfest relation can be questioned for locally less-packed surroundings in which the next nearest neighbor (NNN) contribute significantly to the interference function. Density data support the idea that the packing fraction in the studied amorphous alloys is not too different from that of the crystallized compounds,[22,23] as can be seen in Fig. 9: the density *N* (expressed in mol/cm^3) in the amorphous alloys is only 10% to 12% smaller than expected from a linear extrapolation between pure *M* and Sn crystalline metals and than the densest intermediate phases ($FeSn_2$ and $CoSn_2$, *C* 16 structure), and only 3% to 4% smaller than in the less dense *B* 35 phases (FeSn or CoSn).

In conclusion it seems reasonable to assume that the same kind of short-range order (SRO) occurs in the amorphous, liquid or crystalline states of these M_xSn_{1-x} systems. The main ingredients of this SRO would be as follows:

(i) *M* atoms with a close-packed surrounding.

(ii) $d_{Sn\text{-}Sn}>d_{M\text{-}Sn}=d_{M\text{-}M}$ which would rule out any hard-spheres model.

(iii) Two different tin "sites", Sn_I and Sn_{II} with Sn_{II} at the center of a six-iron-atom trigonal prism similar to that of the model proposed by Gaskell[24] for M_3X (X = metalloid) amorphous alloys, and Sn_I with a more flexible surrounding but including tin atoms.

(iv) Quite a large value of the density. Differen-

TABLE II. Local surrounding (coordination number, type of atom and distances) for some intermediate compounds of the Fe-Sn system.

Compound Atom	FeSn (B 35)	Fe_3Sn (D0 19)	Fe_3Sn_2
M(Fe)	4 Fe at 2.65 Å 6 Sn at 2.65 Å or 2.70 Å	8 Fe at 2.62–2.84 Å 4 Sn at 2.73 Å	6 Fe at 2.59–2.75 Å 5 Sn at 2.68–2.80 Å
Sn_I	6 Fe at 2.65 Å	12 Fe at 2.73 Å	9 Fe at 2.68–2.80 Å
Sn_{II}	6 Fe at 2.70 Å 3 Sn at 3.06 Å		6 Fe at 2.73 Å 3 Sn at 3.09 Å

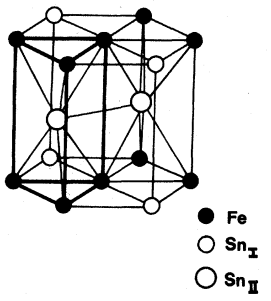

FIG. 8. Structural element of the M-Sn crystalline systems.

tiation of liquid, amorphous, and crystalline states would occur at medium and long range distance through more or less regular connectivities between the trigonal prism structural units: few or no connectivities in the liquid, a number of almost randomly distributed connectivities in the amorphous state, and the good regular connectivities in the crystal. The Co_3Sn_2 and Ni_3Sn_2 compounds in their high-temperature phase and Fe_5Sn_3 which include some disorder might be considered as a first step from the crystal toward the amorphous state.

V. ELECTRICAL TRANSPORT PROPERTIES

A. Experimental data

Figure 10 shows the composition dependences of the as-quenched resistivity $\rho_0(x)$ and the TCR coefficient $\alpha(x)$ as measured at $T=200$ K after thermal annealing of the samples up to 300 K. The $\rho_0(x)$ curves reach maxima $\rho_0^{\max}$ at $x=x_0$ and $\alpha(x)$ have minimum values $\alpha_{\min}$ at $x=x_\alpha$ as reported in Table III. The α values are mostly negative except for Fe_xSn_{1-x} and Co_xSn_{1-x} alloys of the iron-rich or cobalt-rich side.

A direct comparison of these data with measurements carried out in the same liquid systems would have been very interesting, but the $\rho_0(x)$ values are only available for the Co-Sn and Ni-Sn liquid alloys,[25] and Fe and Sn are not miscible in the liquid state. Then, taking opportunity of a small difference of the electrical resistivities as measured in the M-Sn and M-Ge liquid alloys, the present data will be compared to electrical transport properties of the Fe-Ge, Co-Ge, and Ni-Ge liquid systems which have been more completely investigated[26] (see Fig. 11).

A direct comparison of the slopes $(d\rho/dT)(x)$ values is made in Fig. 12 which shows that the

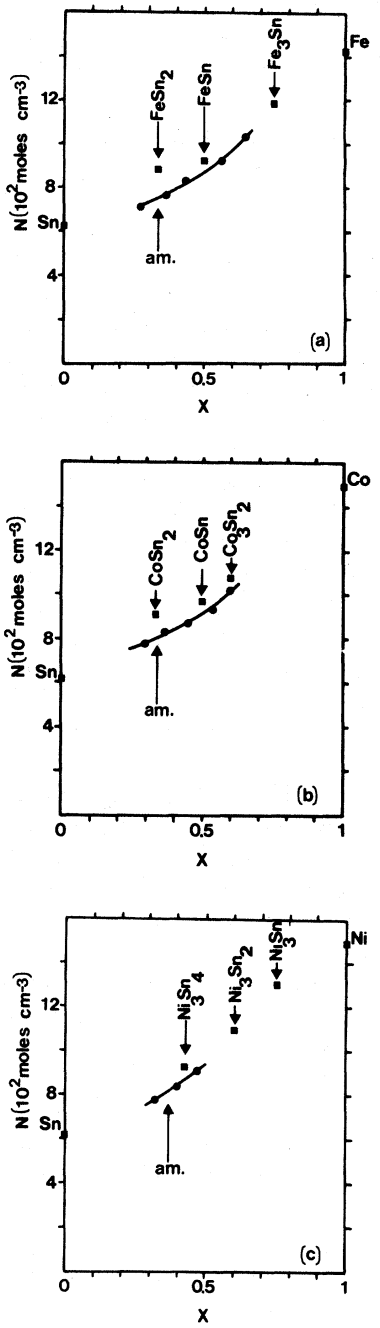

FIG. 9. Density data of the M_xSn_{1-x} amorphous alloys [$M=$ (a) Fe, (b) Co, (c) Ni] and equilibrium phases. [Sn→white Sn; Co→Co (hcp)].

temperature dependences in the whole compositional range are quite similar in liquid M-Ge and amorphous M-Sn alloys. Then, the 0-K resistivity of each amorphous or liquid alloy has been calculated through a linear extrapolation:

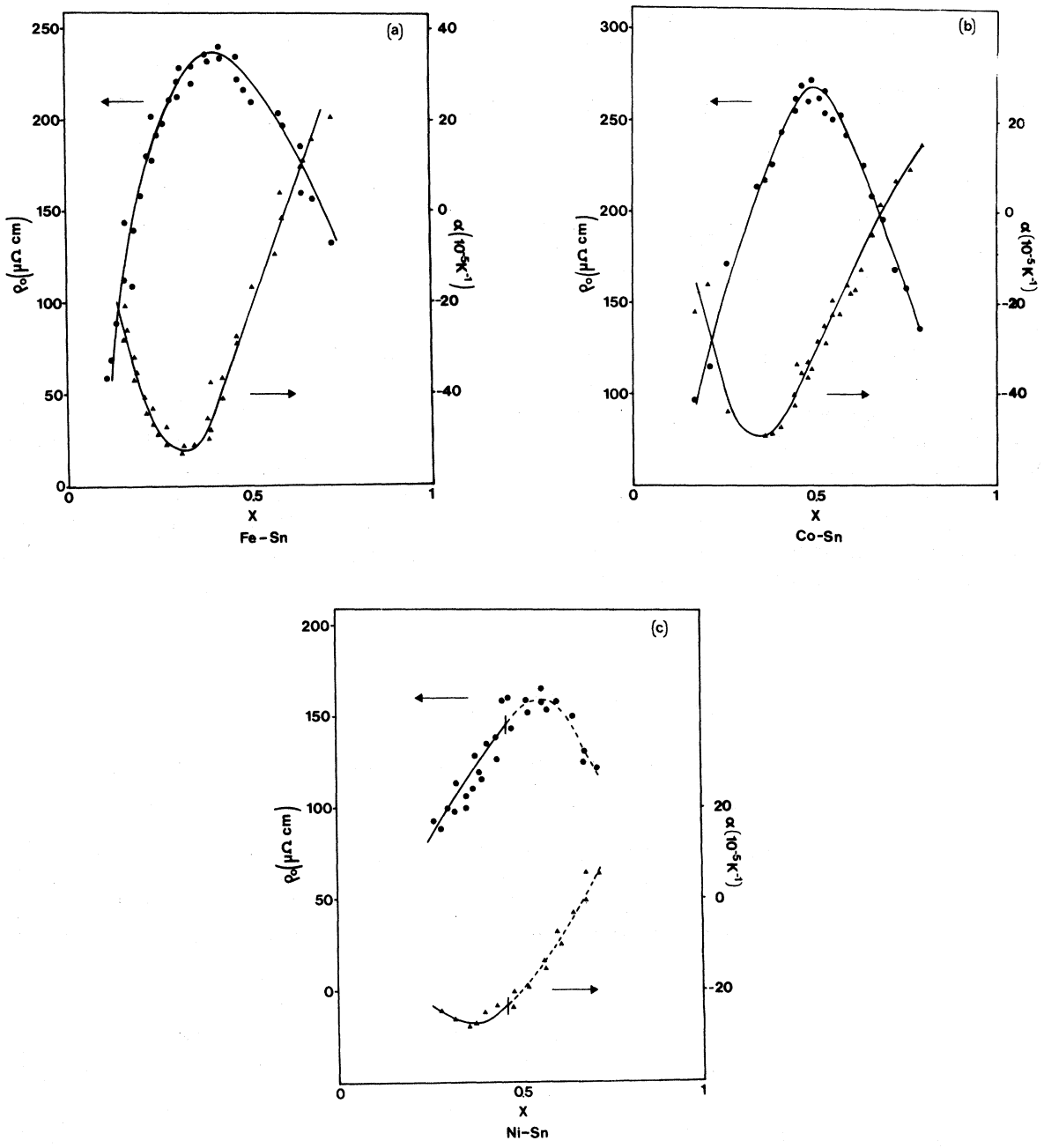

FIG. 10. Electrical transport data of the M_xSn_{1-x} amorphous alloys [$\rho_0(x)$ and $\alpha(x)$]. [$M=$ (a) Fe, (b) Co, (c) Ni]. Dashed line: Amorphous pool with small crystals.

$$\rho(0\ \mathrm{K})=\rho(T)-T\left[\frac{d\rho}{dT}\right]_T .$$

As clearly seen in Fig. 13, the $\rho(0\ \mathrm{K},x)$ curves are quite the same for corresponding liquid and amorphous systems. This is precise evidence for the well-known possibility that the electrical resistivity of an amorphous alloy may be just an extrapolation of the liquid behavior toward low temperatures. To our knowledge, it has never been reported over such a large compositional range and is consistent with the SRO, being the same in liquid and amorphous states over a distance of the order of the electronic mean free path.

TABLE III. Characteristics of the maxima in the resistivity curves and of the minima in the TCR curves for M_xSn_{1-x} amorphous alloys.

Alloys	ρ_0^{max} ($\mu\Omega$ cm)	x_0	$\alpha_{min}(\times 10^4)$	x_α
Fe_xSn_{1-x}	235	0.41	−5.2	0.32
Co_xSn_{1-x}	265	0.48	−4.7	0.35
Ni_xSn_{1-x}	out of the stability range			
	155	0.56	−2.9	0.37

B. Nearly-free-electron model of the resistivity

Similarities of $\rho_0(x)$ and $\alpha(x)$ curves for amorphous and liquid alloys suggest an interpretation of the experimental data in terms of the nearly-free electron model of Ziman[27] extended to liquid transition metals.[28] The resistivity, calculated through the Boltzmann transport equation and neglecting all multiple two-site scattering corrections is given in a pure liquid by

$$\rho=\frac{12\pi\Omega_0}{\hbar e^2 v_F^2}\int_0^1 d\left[\frac{K}{2k_F}\right]\left[\frac{K}{2k_F}\right]^3 S(K)\,|\,t(k_1,k_2)\,|^2 ,$$

in which $S(K)$ is the structure factor given by the experimental interference function, $t(k_1,k_2)$ is the single-site scattering matrix and v_F, k_F refer to Fermi velocity and Fermi sphere radius. Using a muffin-tin approximation $t(k_1,k_2)$ is expressed in terms of the phase shifts η_l through the equation[29,30]

$$t(k_1,k_2)=-\frac{4\pi}{\Omega_0 E_F^{1/2}}\sum_l (2l+1)\sin\eta_l \exp(i\eta_l)P_l(\cos\theta) .$$

In binary alloys the product $S(k)t^2$ in the ρ expression must be replaced by:

$$xt_1^2(1-x+xS_{11})+(1-x)t_2^2[x+(1-x)S_{22}]+x(1-x)(t_1^*t_2+t_1t_2^*)(S_{12}-1) ,$$

in which the subscripts 1 and 2 refer to the alloy components, and S_{ij} are the partial structure factors. In fact, it has been shown that when a transition metal is present its scattering matrix masters the resistivity behavior especially through the η_2 term contribution. This term decreases from Fe to Co and Ni.

On the other hand, backscattering of electrons at the Fermi level ($K=2k_F$) has a major contribution to

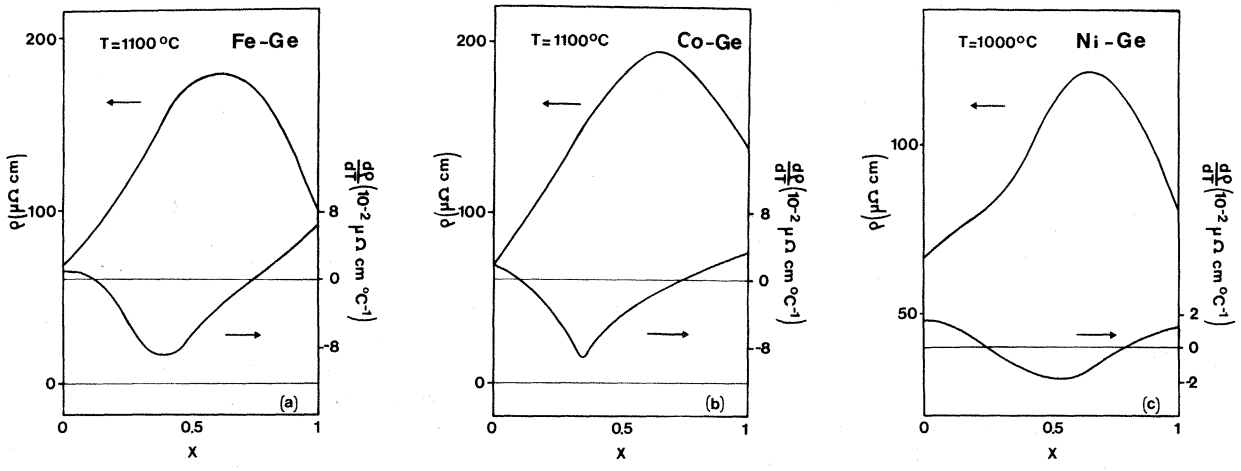

FIG. 11. Electrical transport data of the M_xGe_{1-x} liquid alloys [M = (a) Fe, (b) Co, (c) Ni].

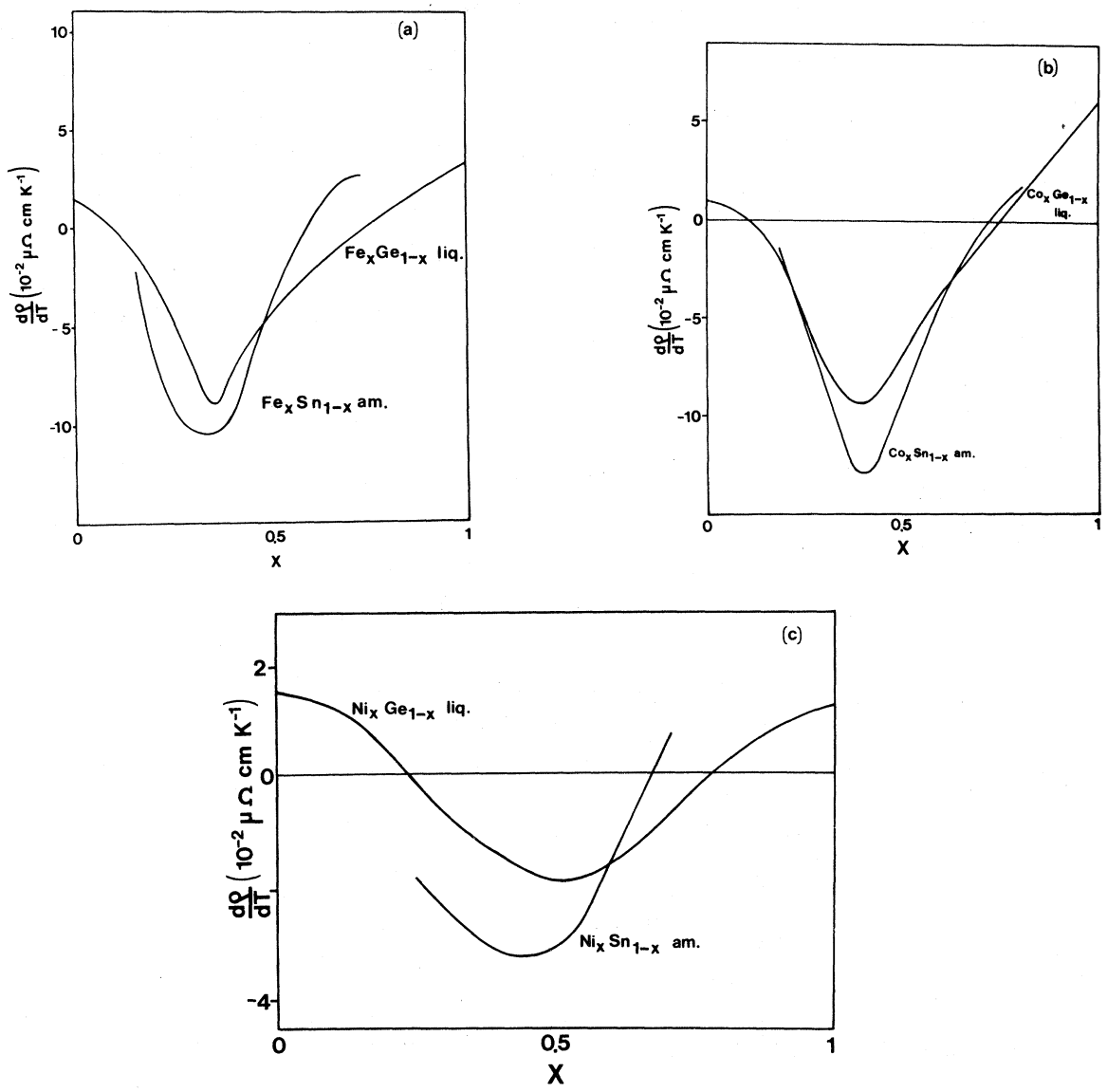

FIG. 12. Comparison of the slopes $d\rho/dT$ of the M_xSn_{1-x} amorphous alloys (measured at 200 K) and of the M_xGe_{1-x} liquid alloys (measured at about 1000 or 1100 °C). [M = (a) Fe, (b) Co, (c) Ni].

the resistivity through the factor $(K/2k_F)^3$ in the integral. Then a good approximation for the resistivity formula would be[31]

$$\rho=\frac{30(\pi^3\hbar^3)}{m^*e^2k_F^2E_F\Omega(x)}\sin^2\eta_2(E_F)[x(1-x)+x^2S_{M-M}(2k_F)]\ ,$$

The main qualitative features of this formula consistent with the present data are as follows.

(i) The resistivity must be maximum for the alloys whose composition corresponds to an electronic density such as $2k_F$ at the position of the maximum of the M-M partial interference function.

(ii) If x_{max} is the composition which corresponds to this maximum resistivity and if $S_{max}=4$,[32] the value of the maximum resistivity changes from one alloy to the other should be given by

$$[x_{max}(1-x_{max})+4x_{max}^2]\sin^2\eta_2=\rho_0^{max}(M)\ ,$$

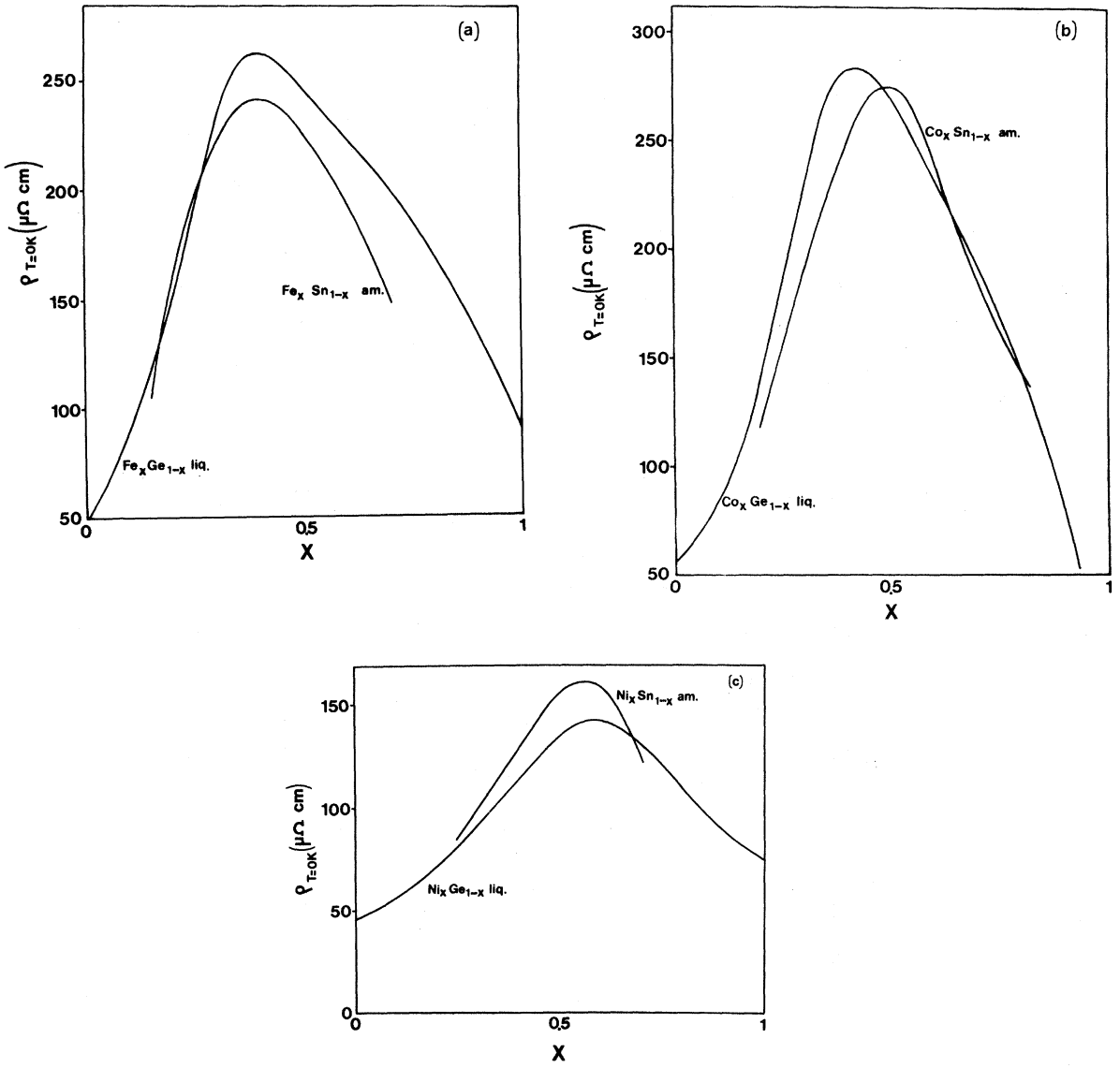

FIG. 13. Resistivity data extrapolated to 0 K as explained in the text.

and should decrease from Fe to Co and Ni in that order (see data in Table III).

(iii) As the resistivity formula does not include physical parameters of the Ge or Sn elements, there is no way to distinguish the M-Ge and M-Sn systems from that point of view. Thus the approximation should be good enough for M-rich alloys and even not too bad on the other side of the compositional range since the electrical resistivity of Ge and Sn liquid are not too different (60 and 48 $\mu\Omega$ cm, respectively[33]).

Calculated values of $2k_F$ through the formula

$$k_F^3 = 3\pi^2[xZ_M N + (1-x)Z_{Sn}N]$$

(in which N is the experimental density shown in Fig. 9, and $Z_M = 1$ and $Z_{Sn} = 4$ are the valences of the transition metal and tin atoms respectively[30]) are compared to K_1 in Fig. 14. The condition $2k_F = K_1$ corresponds, indeed, to larger concentrations of the transition metal than the ones at which $\rho_0(x)$ are maximum but the order of magnitude is acceptable, and on the other hand, there is no possible intersection of K_1' [the Sn-Sn correlation peak in $S(K)$] with $2k_F(x)$ thus confirming the leading

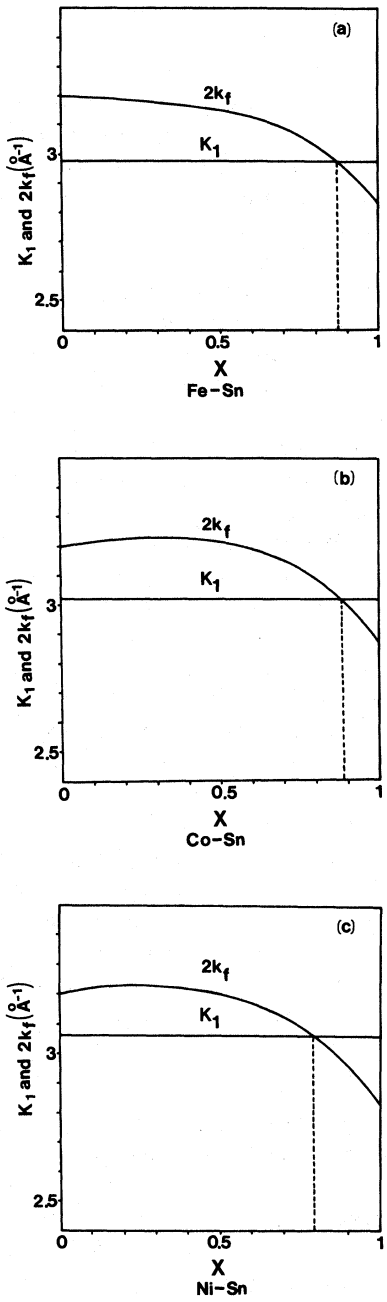

FIG. 14. Comparison of the Fermi sphere diameter to the first peak position of the partial *M-M* interference functions (a) Fe-Sn, (b) Co-Sn, (c) Ni-Sn.

role of the *M* atoms in the resistivity behavior. Any attempt to go further in using this model for a more quantitative interpretation of the data would be quite out of reason.[34] One may speculate that charge tranfer would result in a significant decrease of $x_{\max}$ (Ref. 35) and it could be interesting to make this point more precise by systematic measurement of the isomershift with the Mössbauer spectroscopy of the ^{119}Sn isotope.

C. Temperature dependence of the electrical resistivity

The usual way of accounting for the temperature dependence of the electrical resistivity in liquid and amorphous metals[36–38] is to introduce the atomic excitations in the structure factor, assuming that the scattering matrix $t(k_1,k_2)$ keeps a constant value. Then, if the thermal excitation of the atoms are described in a Debye approximation:

$$S_{ij}^{T}(k)=1+[S_{ij}^{0}(k)-1]e^{-2[W(T)-W(0)]}$$

in which e^{-2W} is the usual Debye-Waller factor (subscripts T and 0 in S or W refer to the actual temperature and the 0-K limit, respectively) with

$$W(0)=\frac{3\hbar^2k^2}{8Mk_B\Theta_D}$$

and

$$W(T)\simeq W(0)+4W(0)\frac{T}{\Theta_D} \quad \text{if } T>>\Theta_D ,$$

where Θ_D is the Debye temperature.

Assuming that the exponential functions in $S_{ij}^{T}(k)$ can be reasonably replaced by their first-order approximation results in

$$S_{ij}^{T}(k)=1+[S_{ij}^{0}(k)-1]\left[1-8W(0)\frac{T}{\Theta_D}\right]$$

and

$$\rho^{\max}(T)=\rho^{\max}(0)\left[1-10\frac{T}{\Theta_D^2}\right],$$

$$\alpha_{\min}\simeq-\frac{10}{\Theta_D^2} .$$

Thus, the TCR $\alpha(T)$ can be positive or negative, depending on the value of S_{ij}^{0} $(2k_F)$ with respect to 1, with the largest negative value being reached when $2k_F=K_1$. Using data from Table III and the above theoretical expression of $\alpha_{\min}$ gives Θ_D(Fe-Sn)=140 K, Θ_D(Co-Sn)=145 K, Θ_D(Ni-Sn)=190 K.

These values are of the same magnitude as the one reported for the Cu-Sn amorphous system[39] (Θ_D=150 K) but are significantly smaller than the Debye temperature measured in the pure crystalline

component metals: Θ_D(Fe)=467 K, Θ_D(Co)=445 K, Θ_D(Ni)=450 K, Θ_D(Cu)=343 K, Θ_D(Sn)=200 K.

The unexpected observed increase from Fe to Co and Ni alloys might come from a temperature dependence of the t matrix which is probably sensitive to the broadening of the Fermi level as already mentioned by Mott.[40]

VI. A GENERAL DISCUSSION ABOUT FORMING ABILITY AND STABILITY CRITERIA IN AMORPHOUS METALS: CONTRIBUTION OF THIS PAPER TO THESE CRITERIA

In this section, the stability of the amorphous alloys studied in this paper will be discussed in terms of usually accepted criteria: size effect, existence of covalent bondings, particular composition with respect to the equilibrium phase diagram, electronic criterion, or formation enthalpy of defects such as vacancies.

A. Size effect

Since early work in amorphous alloys, it has been predicted[41] that an atomic size difference of constituents greater than 10% should exist as a requirement for the formation of glassy state. Even if, in fact, amorphous states have been produced which do not fulfill this size criterion,[13] one can understand that it is just the counterbalance of the size effect criterion to obtain crystalline solid solution: If chemical disorder is imposed to a mixture of tiny and huge atoms, long-range order is rejected by the assembly.[42]

Furthermore, in computer calculations or structure models, filling spaces between random-packed hard spheres[43] by atoms with small radii could result in closer packing than that with atoms having uniform, hard sphere radii,[44,45] with (of course) restrictions over the acceptable composition ranges.[46]

In terms of such a size criterion, the M=Fe, Co, Ni, and Sn atoms are indeed good candidates to produce amorphous systems since the Goldschmidt radii for Sn, Fe, Co, and Ni are 1.62, 1.27, 1.25, and 1.25 Å, respectively[47]; that is a size effect of about 25%. However, a Polk model[44] of the structure is unacceptable to account for the large ranges of forming ability observed here. It is worth noting that stability differences measured among the three systems shall not result from size effects.

B. Existence of covalent bondings

Metalloids have indeed a great tendency to produce amorphous phases. However, it is also noticeable that alloys mixed only with metals can form amorphous materials [Ca-Zn (Ref. 48), Cu-Zr (Ref. 49)]. The admitted role of metalloid or semimetal elements as glass-forming partners has been explained by blocking of the atomic diffusion due to the bonding structures and the atomic mobility compared to those resulting from isotropic metallic bonding: Pure amorphous silicon[50] crystallizes at a much greater temperature than amorphous metals.[51] In M_xSn_{1-x} amorphous alloys, it would be an appealing assumption to consider the tin atoms as the glass-forming partners. However, this point is strongly questionable because of a pure metallic behavior of the electrical transport properties observed in the whole compositional range of stability. There is here no evidence of the metal-insulator-like transition which has been found elsewhere in amorphous systems such as Au-Si,[9] Fe-Si,[13] Fe-Ge,[52] or Sb-Au.[53] Such a pure metallic behavior has to be compared to that reported in Cu-Sn (Ref. 54) or Au-Sn (Ref. 55) amorphous alloys.

A contradictory remark in that respect will concern the crystalline equilibrium phases, particularly the equi-atomic Fe-Sn and Co-Sn compounds which exhibit the same B 35 structure as Fe-S,Cr-Sb,Mn-Te, . . . , where the metalloid character of S,Sb,Te, . . . cannot be questioned and introduces clear superexchange phenomena.[56]

C. Compositional ranges of forming ability and equilibrium phase diagrams

Explanation of the forming ability for glass systems in terms of the equilibrium phase diagrams has given rise to at least three different kinds of criteria:

(1) The glass formation would be favored at deep eutectic compositions.[57]

(2) Solid solution compositional ranges must be avoided.[42]

(3) Good candidate compositions should correspond to crystalline stable or metastable stoichiometric compounds[24] or to complex phases having large primary cells.[58]

In Fig. 15, equilibrium phase diagrams[21] of the (Fe,Co,Ni)-Sn systems are shown along with the forming ability ranges of composition measured for

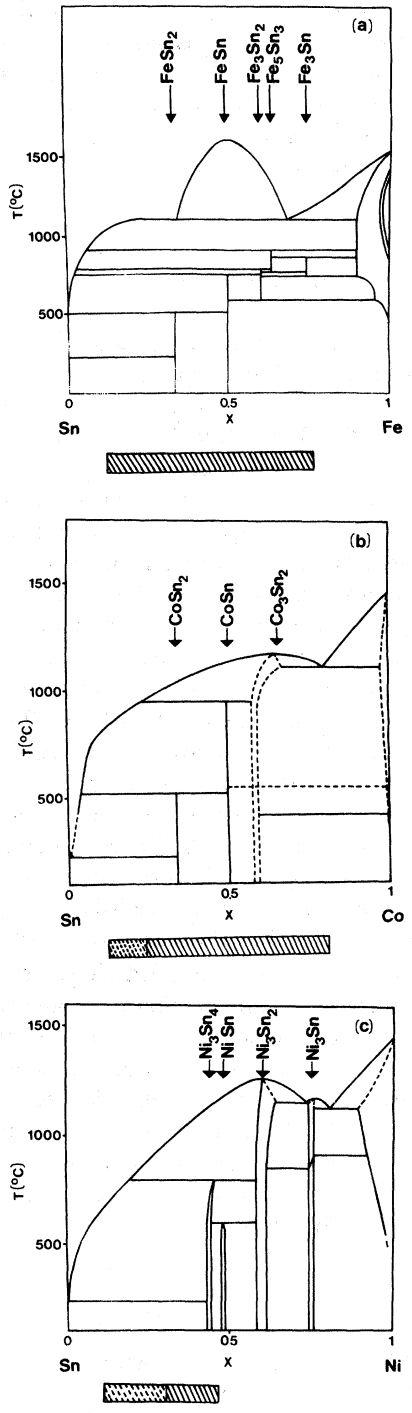

FIG. 15. Equilibrium phase diagrams of the M-Sn systems with the ability range of amorphous alloys formation.

the corresponding amorphous alloys: There is no deep eutectic—the forming ability ranges are far from the extreme solid solutions but include stable intermetallic compounds.

The *deep eutectic criterion,* which might be generalized as a low liquidus temperature criterion, is in fact typical of the amorphous alloys obtained from fast quenching of the liquid. In such cases the critical temperature range between solidification and glass formation is sufficiently reduced [$T_g/T_m > 0.45$ (Ref. 59)] for by-passing crystallization relatively easily. In the present M_xSn_{1-x} alloys, the existence of a relatively low liquidus temperature of a deep eutectic is not a necessary condition in obtaining amorphous states since the kinetic problems of crystallization are mostly avoided in evaporation methods.

The *out of solid solution criterion* introduced by Mader *et al.*[42] applies, for instance, to Fe_xAu_{1-x} amorphous alloys[60] and has in fact something to do with the size effect criterion as previously explained. It is a kind of extension of the Hume-Rothery rules[61] to amorphous systems. This criterion fully applies to the present M_xSn_{1-x} alloys.

Correlations between the existence of intermediate phases and the forming ability composition range. In the three systems, several intermediate phases occur and one can observe a correlation between the existence of stoichiometric intermediate phases and the forming ability of amorphous alloys. The ability range is the widest for the systems containing stoichiometric phases, Fe-Sn and Co-Sn. For Ni-Sn, the nonstoichiometric crystalline structures would accommodate chemical disorder. This hypothesis with the "out of solid solution" criterion would constitute a minimum disorder principle in condensed metallic matter: During the condensation, chemical disorder is imposed and an amorphous phase occurs if it cannot be accommodated by a crystalline structure.

D. Stability of the amorphous state and vacancy formation in the corresponding crystalline alloys

Buschow *et al.*[62,63] suggest that crystallization needs vacancies to occur and then the crystallization temperature should increase with the formation enthalpy of the easiest obtainable vacancy. In the Buschow model, the formation enthalpy is calculated using a semiempirical theory proposed by Miedema.[64,65] The formation enthalpy of a vacancy is obtained as the surface enthalpy of a hole of the size of an atom. The smaller the hole size and the surface enthalpy of the surrounding atoms, the smaller the formation enthalpy of the vacancy. In

M-Sn alloys the M vacancy is more easily formed because the M atoms are smaller than the Sn atoms and are mostly surrounded by Sn atoms whose surface enthalpy is the smallest (Table IV). Such an easy formation of the M vacancy is consistent with the occurrence of $B\,8_2$ structures for some of the M-Sn crystalline phases.

In alloys Miedema has calculated the formation enthalpy of a vacancy. In the present case, the Miedema formula applied to the M vacancy can be written:

$$\Delta H_{1V}^{M}(\text{alloy}) = C\Delta H_{1V}^{M} + (1-C)\left[\frac{V_M}{V_{\text{Sn}}}\right]^{5/6}\Delta H_{1V}^{\text{Sn}},$$

in which ΔH_{1V} and V are the formation enthalpies and molecular volumes in each pure constituent and

$$C = xV_M^{2/3}/[xV_M^{2/3} + (1-x)V_{\text{Sn}}^{2/3}]$$

is the "mean surface concentration" of the M atoms in the alloy. The compositional dependence of the ΔH_{1V}^{M} (am-alloy) is shown in Fig. 16. It can be seen that ΔH_{1V}^{M} increases with the M concentration, for a given system and from Ni to Co to Fe for a given composition. As pictured in Fig. 17, the crystallization temperatures T_{cr} increase with ΔH_{1V}^{M}. The experimental data cloud is reasonably gathering near the linear fit reported by Buschow[62] in the study of M-Hf, M-Y, Fe-Th, Ni-Th, Ni-Nb, and Zn-Mg amorphous alloys. In this paper, data for Co-Sn alloys are above while data for Fe-Sn and Ni-Sn are below this linear fit. Thus, a correlation between T_{cr} and ΔH_{1V}^{M} may be obviously stated but the Miedema model does not interpret correctly the relatively great crystallization temperature of the Co alloys compared to those of the Fe alloys and does not take into account chemical SRO effect.

Such an empirical correlation between T_{cr} and ΔH_{1V} is somewhat similar, basically, to that usually observed between the melting point and ΔH_{1V}: Crystallization as well as melting requires atomic displacements and then vacancies or vacancylike defects. In each system, T_{cr} increases with the liquidus temperature T_l.

E. Electronic criterion

Some of the obtained amorphous alloys have compositions which correspond roughly to $2k_F \simeq K_p$ (K_p first maximum in the interference function). Nagel and Tauc[66] have suggested that it should be due to the existence of a pseudogap at $(\hbar^2/2m)(K_p/2)^2$ in the electronic state density. A maximum resistance against crystallization would occur when the Fermi level falls in this pseudogap. An alternative explanation has been proposed by Hafner[48,67] and Beck *et al.*[68]: The ionic pseudopotential in alloys having an oscillating part in $2k_F r$, and the structure will be stable if the neighboring atoms are into the attractive minima of this potential, such as $2k_F \simeq K_p$. These nearly-free-electron approaches cannot reasonably apply to the $M_x\text{Sn}_{1-x}$ amorphous alloys, but are of interest because of their relation to the Faber-Ziman model of electrical transport. Thus the criterion $2k_F \simeq K_p$ (here $K_p = K_1$) would simultaneously correspond to $\rho_0^{\max}$, $\alpha_{\min}$, and $T_{\text{cr}}^{\max}$. This is not truly observed in the present work but the studied alloys are mostly produced in the negative region of α, and the greater $\rho^{\max}$, the higher T_{cr} for a given composition. The common physical origin of such correlations between stability, large electrical resistivity, and negative TCR is still unclear, but it has been shown here that this correlation is not closely linked with the occurrence of a deep eutectic as suggested by Buschow.[69]

TABLE IV. Vacancy formation data in Fe, Co, Ni, and Sn as compared to calculated values from the Miedema model (Ref. 64). Surface enthalpy values are also shown.

Pure metal	$\Delta H_{1V}^{\text{calc}}$ (kJ/mole)	$\Delta H_{1V}^{\text{expt}}$	Surface enthalpy (J/m^2)
Fe	139	140	2.55
Co	112	120	2.55
Ni	104	135	2.45
Sn	54	50	0.71

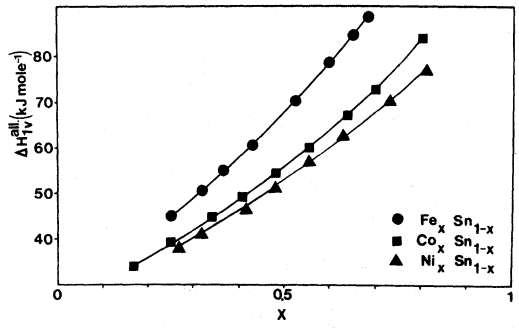

FIG. 16. Compositional dependence of the formation enthalpy of vacancies in M-Sn alloys.

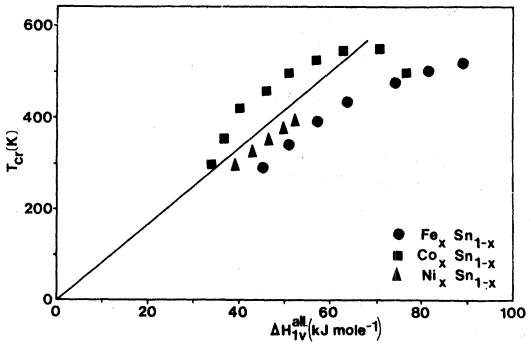

FIG. 17. Correlation of ΔH_{1V} and T_{cr} in amorphous M-Sn alloys. The straight line corresponds to Buschow's fit.

VII. CONCLUSION

Amorphous alloys of the Fe_xSn_{1-x}, Co_xSn_{1-x}, and Ni_xSn_{1-x} systems have been obtained by a vapor quenching technique in quite large ranges of composition. Structural investigations and electrical resistivity measurements have suggested that short-range order might be practically the same in the crystalline, amorphous and liquid states with, in particular, the existence of structural units made of one Sn atom at the center of six iron trigonal prisms and equal distances between M-M and M-Sn atoms. Structural differentiation of liquid, glass, and crystal would arise from the nature of the connectivity regions between these structural units.

A detailed analysis of the stability and forming ability data has led to conclusions that may be summarized in a kind of *minimum disorder principle in condensed metallic matter.* On one hand, when fast quenching techniques are used in an attempt to prepare disordered alloys, this minimum disorder principle would result in the appearance of a fairly well-defined SRO, typical of the system. On the other hand, medium- and long-range chemical disorder would go along with topological disorder only when there is no possibilities for a crystalline phase to accommodate such a disorder.

Finally, it must be pointed out that stability and forming ability, although both are notions probably linked to atomic transport phenomena, have to be considered separately.

The Miedema model approximatively gives the formation enthalpy of the single vacancy and an estimation of the crystallization temperature. This point is consistent with the correlation between crystallization and liquidus temperatures.

Some other experimental investigations of these M_xSn_{1-x} amorphous alloys are still in progress in our laboratory, especially concerning those magnetic properties. Results will be given in a subsequent paper.

[1]B. C. Giessen and S. Whang, J. Phys. (Paris) 41, C8-95 (1980).
[2]E. Hornbogen and I. Schmidt, in *Liquid and Amorphous Metals,* edited by Lüscher and Coufal (Sijthoff and Noordhoff, Aljhen aan deu Rijn, 1980) p. 353.
[3]L. Holland, *Vacuum Deposition of Thin Films* (Chapman and Hall, London, 1961), 4th Ed. p. 141.
[4]P. B. Hirsch, A. Howie, R. B. Nicholson, D. W. Pashley, and M. J. Whelan, *Electron Microscopy of Thin Crystals* (Butterworths, London, 1965).
[5]S. Fujime, Jpn. J. Appl. Phys. 5, 1029 (1966).
[6]M. L. Theye, M. Gandais, and S. Fisson, Phys. Status Solidi A 17, 643 (1973).
[7]*International Tables for X-ray Crystallography* (Kynoch, Birmingham, England, 1974).
[8]P. K. Leung and J. G. Wright, Philos. Mag. 30, 185 (1974).
[9]P. Mangin, G. Marchal, C. Mourey, and C. Janot, Phys. Rev. B 21, 3047 (1980).
[10]K. H. Behrndt, J. Vac. Sci. Technol. 8, 622 (1971).
[11]S. Tolansky, *Multiple Beam Interferometry of Surfaces and Films* (Oxford University Press, London, 1948), p. 135.
[12]G. Marchal, B. Rodmacq, P. Mangin, M. Piecuch, and

C. Janot, Mater. Sci. Eng. 36, 11 (1978).
[13]P. Mangin, G. Marchal, B. Rodmacq, and C. Janot, Philos. Mag. 36, 643 (1977).
[14]D. Korn, H. Pfeifle, and G. Zibold, Z. Phys. 270, 195 (1974).
[15]B. Rodmacq, M. Piecuch, C. Janot, G. Marchal, and P. Mangin, Phys. Rev. B 21, 1911 (1980).
[16]D. M. North and C. N. J. Wagner, Phys. Chem. Liq. 2, 87 (1970).
[17]H. Leitz, Z. Phys. B 40, 65 (1980).
[18]J. E. Enderby, D. M. North, and P. A. Egelstaff, Philos. Mag. 14, 961 (1966).
[19]C. N. J. Wagner, in *Liquid Metals,* edited by S. Z. Beer (Dekker, New York, 1972).
[20]D. M. North and C. N. J. Wagner, Acta Crystallog. 25A, S16 (1969).
[21]M. Hansen, *Constitution of Binary Alloys,* 2nd Edition (McGraw-Hill, New York, 1958).
[22]C. Djega-Mariadassou, Ph.D. thesis, Faculté des Sciences, Orsay, 1970 (unpublished).
[23]B. Malaman, Ph.D. thesis, Faculté des Sciences, Nancy, 1978 (unpublished).
[24]P. H. Gaskell, J. Non-Cryst. Solids 32, 207 (1979).
[25]H. J. Güntherodt and H. U. Künzi, Phys. Condens. Matt. 16, 117 (1973).
[26]B. Busch, H. J. Güntherodt, H. U. Künzi, H. A. Meier, and L. Schlapbach, Mater. Res. Bull. 5, 567 (1970).
[27]J. M. Ziman, Philos. Mag. 6, 1013 (1961).
[28]R. Evans, H. J. Güntherodt, H. U. Künzi, and A. Zimmermann, Phys. Lett. 38A, 151 (1972).
[29]O. Dreirach, R. Evans, H. J. Güntherodt, and H. U. Künzi, J. Phys. F 2, 709 (1972).
[30]K. Hirata, Y. Waseda, A. Jain, and R. Srivastava, J. Phys. F 7, 419 (1977).
[31]R. Evans, D. A. Greenwood, and P. Lloyd, Phys. Lett. 35A, 57 (1971).
[32]Y. Waseda, H. Okazaki, and P. Masumoto, J. Mater. Sci. 12, 1927 (1977).
[33]N. E. Cusack, Rep. Prog. Phys. 26, 361 (1963).
[34]M. Piecuch, C. Janot and G. Marchal, J. Phys. (Paris) 41, C1-251 (1980).
[35]E. Esposito, H. Ehrenreich, and G. D. Gelatt, Phys. Rev. B 18, 3913 (1978).
[36]S. R. Nagel, Phys. Rev. B 16, 1649 (1977).
[37]P. J. Cote and V. Meisel, Phys. Rev. Lett. 39, 102 (1977).
[38]P. J. Cote, Solid State Commun. 18, 1311 (1976).
[39]K. Froböse and J. Jäckle, J. Phys. F 7, 2331 (1977).
[40]N. F. Mott, Philos. Mag. 13, 989 (1966).
[41]K. H. Behrndt, J. Vac. Sci. Technol. 7, 385 (1970).
[42]S. Mader and A. S. Nowick, Appl. Phys. Lett. 7, 57 (1965).
[43]J. D. Bernal, Nature (London) 185, 68 (1960).
[44]D. E. Polk, Acta Metall. 20, 485 (1972).
[45]J. F. Sadoc, J. Dixmier, and A. Guinier, J. Non-Cryst. Solids 12, 46 (1973).
[46]R. Yamamoto, T. Mihara, and M. Doyama, Phys. Status Solidi A 50, 165 (1978).
[47]*Metals Reference Book,* 5th ed., edited by C. J. Smithells (Butterworths, London, 1978), p. 100.
[48]J. Hafner, Phys. Rev. B 21, 406 (1980).
[49]R. Ray, B. C. Giessen, and N. G. Grandt, Scripta Metall. 2, 357 (1968).
[50]U. Köster, Phys. Status Solidi A 48, 313 (1978).
[51]M. R. Bennett and J. G. Wright, Phys. Status Solidi A 13, 135 (1972).
[52]O. Massenet, H. Daver, and J. Geneste, J. Phys. (Paris) 35, C4-279 (1974).
[53]P. Häussler, W. H. G. Müller, and F. Baumann, Z. Phys. B 35, 67 (1979).
[54]D. Korn, W. Mürer, and G. Zibold, J. Phys. (Paris) 35, C4-257 (1974).
[55]E. Blasberg, D. Korn, and H. Pfeifle, J. Phys. F 9, 1821 (1979).
[56]A. Herpin, *Théorie du Magnétisme* (Presses Universitaires de France, Paris, 1968), p. 611.
[57]W. Klement, R. H. Willens, and P. Duwez, Nature (London) Phys. Sci. 187, 809 (1960).
[58]D. E. Polk and B. G. Giessen, *Metallic Glasses* (American Society for Metals, Cleveland, 1978), p. 1.
[59]M. H. Cohen and D. Turnbull, J. Chem. Phys. 31, 1164 (1959).
[60]G. Marchal, P. Mangin, and C. Janot, Philos. Mag. 32, 1007 (1975).
[61]W. Hume-Rothery, *Phase Stability in Metals and Alloys,* Series in Materials Science and Engineering (McGraw-Hill, New York, 1967), p. 3.
[62]K. H. J. Büschow and N. M. Beekmans, Solid State Comm. 35, 233 (1980).
[63]K. H. J. Büschow, J. Phys. (Paris) 41, C8-559 (1980).
[64]A. R. Miedema, Z. Metallkd. 70, 345 (1979).
[65]A. R. Miedema, P. F. de Chatel, and F. R. de Boer, Physica 100B, 1 (1980).
[66]S. R. Nagel and J. Tauc, Phys. Rev. Lett. 35, 380 (1975).
[67]J. Hafner and L. von Heimendahl, Phys. Rev. Lett. 42, 386 (1979).
[68]H. Beck and R. Oberle, *Rapidly Quenched Metals III* (Metal Society, London, 1978), p. 416.
[69]K. H. J. Büschow and N. M. Beekmans, Phys. Status Solidi A 60, 193 (1980).